atmosphere

MDPI

Article

A Refined Study of Atmospheric Wind Properties in the Beijing Urban Area Based on a 325 m Meteorological Tower

Shi Zhang [1], Bo Li [2,3,*], Giovanni Solari [4], Xinxin Zhang [5] and Xiaoda Xu [6]

1 School of Civil and Transportation Engineering, Beijing University of Civil Engineering and Architecture, No. 1 Zhanlanguan Road, Xicheng District, Beijing 100044, China; zhangshi@bucea.edu.cn
2 School of Civil Engineering, Beijing Jiaotong University, No. 3 Shangyuancun, Haidian District, Beijing 100044, China
3 Beijing's Key Laboratory of Structural Wind Engineering and Urban Wind Environment, No. 3 Shangyuancun, Haidian District, Beijing 100044, China
4 Department of Civil, Chemical and Environmental Engineering, University of Genoa, Via Montallegro, 1, 16145 Genoa, Italy; giovanni.solari@unige.it
5 China Communications Construction Fourth Highway Engineering CO., LTD., No. 91 Jianguo Road, Chaoyang District, Beijing 100022, China; 18121167@bjtu.edu.cn
6 Central Research Institute of Building and Construction CO., LTD. MCC, No. 33 Xitucheng Road, Haidian District, Beijing 100088, China; 13115279@bjtu.edu.cn
* Correspondence: boli@bjtu.edu.cn

Abstract: The urban atmospheric boundary layer (UABL) is complex due to the heterogeneous underlying city surface. The nine anemometers installed at different heights along the 325 m meteorological tower provide an opportunity to carry out a refined study of wind properties in the UABL in central Beijing, China. Based on the recent 5-year high-resolution measured data, in total, 229,488 10-min length segments of wind records related to each anemometer are reliable for further analyses. Accordingly, the statistical properties of the wind speed and direction are first analyzed to present the local wind climate in a comprehensive way. Moreover, the pattern of the wind profiles related to two typical synoptic intense events are illustrated in order to give a preliminary perspective, then the statistical properties corresponding to a series of intense windstorms are described. Here, the deviations in the wind direction occur between 200 m and 280 m of the atmosphere, which might be due to the existence of an Ekman spiral; besides this, the laws of wind profiles based on open terrain are not suitable for the UABL, and the aerodynamic characteristic parameters of the UABL based on vertical stratified structures have to be considered. The results contribute to the establishment of revised models for the wind profile and are useful for the further understanding of the structure of UABL wind.

Keywords: atmospheric boundary layer; field measurement; urban area; wind climate; wind property; wind speed profile

Citation: Zhang, S.; Li, B.; Solari, G.; Zhang, X.; Xu, X. A Refined Study of Atmospheric Wind Properties in the Beijing Urban Area Based on a 325 m Meteorological Tower. *Atmosphere* **2021**, *12*, 786. https://doi.org/10.3390/atmos12060786

Academic Editor: Leonardo Primavera

Received: 29 April 2021
Accepted: 15 June 2021
Published: 18 June 2021

1. Introduction

Wind is one of the most crucial atmospheric phenomena, which tends to cause changes in atmospheric circulation, heat fluxes, surface energy fluxes, and so on [1]. In the atmosphere, with the development of social and technological activities, the underlying surface is much rougher and more complex because engineering structures tend to be higher, larger, and more flexible and complex [2,3]. The understanding of the atmospheric wind field characteristics in relation to local features, especially over complex heterogeneous underlying surfaces, is important for structural wind resistance design and structures' safety and comfort [4–7]. As for the structural wind engineering field, four approaches—theoretical analysis, wind tunnel testing, numerical simulation and field measurement—have been frequently used in the last few decades to investigate the wind field characteristics. Doubtlessly, field measurement is the most direct and reliable in this

framework [2,8]. Therefore, it is of great engineering value and theoretical meaning to analyze the wind field characteristics [9,10].

In order to understand the structure of the wind properties in the atmospheric boundary layer (ABL) and provide wind models for the wind-resistant design of tall and super-tall building structures, it is essential to learn about intense windstorms and their wind speed profiles in the ABL over various types of surface terrains [11]. The literature is rich in contributions that illustrate measured data at various levels, of which the analysis is carried out with the aim of evaluating the wind speed profiles [12,13]. The sensors installed on towers are common instruments to detect data. Besides this, Doppler SODAR (Sound Detection and Ranging) was also applied to the vertical distributions of wind speed characteristics recently [14–16]. It is worth noting that in order to measure the wind speed in the atmosphere by means of a SODAR, it is necessary to rationally set up the SODAR parameters first and accurately measure the Doppler shift [17]. Besides the environmental noise, meteorological factors and turbulence features also affect the accuracy and reliability of the wind velocity measurements. Generally, the results detected by SODAR should be compared with those detected directly by the meteorological instruments in order to correct errors and confirm the accuracy. Therefore, the ultrasonic anemometers are comparatively more effective and reliable.

Regarding this previous research on wind profiles in different countries, almost all of them were carried out over open or suburban terrain, whereas in urban areas, within a couple of kilometers from the site, several changes might occur in the nature of the terrain's surface [18]. Therefore, the traditional laws of wind profiles based on the open flat terrains may be not applicable to the urban atmospheric boundary layer (UABL) wind, which deserves further discussion. In addition, there are very limited reliable measured data in the ABL of urban areas [4]. Accordingly, due to more and more tall and super-tall building structures being built in urban areas throughout the world, it is necessary to collect the local measurement information, especially for the accurate wind-resistant design of structures [19]. Fewer scholars have paid attention to the influence of the Ekman spiral, in which the velocity vector rotates clockwise in direction (in the Northern Hemisphere) and decays exponentially in magnitude with increasing depth [20], which should be considered during the analyses of wind profiles because these deviations of wind direction cannot be ignored any longer in the design of super-tall buildings or gigantic wind turbines, as spiral-shaped wind profiles may impose significant asymmetrical loadings on structures [21]. Furthermore, many of the previous anemometers were installed on existing towers built generally for other purposes, or on poles on the roofs of some buildings without paying enough attention to the wake separation due to the buildings themselves [22–24]. A special meteorological tower with dense and simultaneous measuring points along the height is more effective and professional for learning the spatial and temporal characteristics of the wind speed.

Beijing is the capital of China and one of the largest cities in the world, presenting typical urban terrains and often being hit by strong winds, as shown in Figure 1. The 325 m meteorological tower installed in 1978 is the best observation station to study the urban boundary layer and the strongest urban storms in Beijing city [25]. Accordingly, Li et al. [26] carried out a preliminary study of the wind profile data recorded during one windstorm. Then, they discussed the wind profile by using data obtained from the instrumented tower during a three-year period from 2001 to 2003 [11]. The vane anemometers were adopted for the study and the results presented the wind properties of the past for Beijing. A set of ultra-sonic anemometers was installed at different heights along this tower in 2013, which provide an excellent opportunity to record high-resolution data and learn the present wind field characteristics of the Beijing urban area. Accordingly, Hui et al. [27] studied the non-stationarity and non-Gaussian characteristics of wind speeds based on some selected records measured during the synoptic wind storms. Zhang et al. [25] preliminarily investigated the characteristics of wind profiles related to thunderstorm outflows. Despite these and many other analyses, knowledge of the vertical distribution of

the wind speed in the actual Beijing urban area is still lacking, and a better understanding and quantification of this key information is vital prior to the construction and insurance of building companies, wind energy predictions and exploitation, and so on [18]. This paper contributes to the clarification of such dominant information for structural design wind load. It also adds value for engineering in terms of structure safety and comfort that might ultimately lead to a revision of the Chinese National Load Code.

Figure 1. On 5 May 2017, a tree was blown down by intense wind and hit a car (**a**) https://news.qq.com/a/20170505/025960.htm (accessed on 5 May 2017); a billboard was blown down and injured a pedestrian (**b**) (https://v.qq.com/x/page/n0500nddjni.html? (accessed on 5 May 2017).

In this framework, Section 2 illustrates the main properties of the measurement site and the instruments. Accordingly, Section 3 analyses the statistical properties of the wind speed and direction of the Beijing urban area. Section 4 first investigates the boundary layer wind characteristics of two typical intense synoptic windstorms, then studies the wind profile properties in a statistical environment thanks to anemometers installed at nine different heights. Section 5 summarizes the main conclusions.

2. Measurement Site and Instrumentation

The capital of China, Beijing, lies in the northeast part of the country, with a total area of 16,410.54 square kilometers. The local wind system is dominated by the monsoon-influenced humid continental climate, characterized by hot, humid summers due to the East Asian monsoon, and by cold, windy, dry winters that reflect the influence of the vast Siberian anticyclone. Besides this, thunderstorms also occur frequently, and the average annual number of thunderstorm days in the Beijing area is 35.6. The peak wind speeds produced by thunderstorm events are sometimes relatively stronger than those produced by monsoon winds, while the duration of the thunderstorm outflows is much shorter and the 10-min mean wind speeds are relatively smaller [28]. Therefore, thunderstorm winds are also dominant for the structural design, and their main characteristics related to the wind loading of structures should be considered separately [29]. The Beijing Meteorological Tower, as shown in Figure 2a, located 2.7 km north of Deshengmen, 1 km away from the third ring road of Beijing city, was set up in 1978 for basic scientific research, with a height of 325 m. When it was built, the terrain was flat, with numerous low-rise buildings around the tower. With the rapid development of Beijing, the tower site is now surrounded by some tall buildings with heights between 70 m and 90 m, nearly 500 m away towards the north. There are a few low-rise houses and trees to the east of the tower. Some buildings, including several 60 m high buildings, are about 300 m away from the tower in the southern direction. The area on the west side of the tower is covered by a mixture of trees, low-rise residential houses with the height of about 7 m to 25 m, and roughly 40 m-high buildings [11,30]. The average height of the buildings is about 19.1 m in the range of 4 km $\times$ 4 km around the tower, and it is 18.3 m in the range of 20 km $\times$ 20 km. The object characteristic parameters are shown in Table 1. According to the Chinese National Load Code [31], the site around the tower can be regarded as terrain C (urban area).

Figure 2. Mesh grid of the topographic model satellite image of the landforms around the 325 m meteorological tower in Beijing in 2020 (**a**), and a picture of the tower (**b**).

Table 1. The parameters of the land and buildings around the tower.

Considered Area		4 km × 4 km	20 km × 20 km	60 km × 60 km
Average building height (m)		19.1	18.3	/
Percentage of impervious surface area (%)	Building	68.3	64.6	24.1
	Roads, parking lots, etc.	20.0	13.7	
Percentage of permeable surface area (%)	Grass, trees, etc.	11.7	21.7	75.9

In total, the tower has 11 three-axial WindMaster Pro ultrasonic anemometers produced by GILL Instruments Limited, UK, with a sampling rate of 10 Hz, mounted at nine heights—namely 8 m, 16 m, 32 m, 47 m, 64 m, 80 m, 140 m, 200 m and 280 m, respectively—along the tower, as shown in the Figure 2b. These record the information of the wind speed and temperature continuously. At 32 m and 64 m, two ultrasonic anemometers are installed at the same height and different directions in order to validate the measured fluctuating speeds. The measured data are first averaged within each 10 min interval and compared with the cup-type anemometer data in order to check the reliability before further analyses [11,32,33]. Besides this, in order to avoid the interference effects of the tower on the measured data, the ultrasonic anemometers are fixed 1.5 m away from the tower towards the north, which is in the upwind direction of the tower during the dominant synoptic wind in Beijing in winter and spring.

As shown in Figure 3, the anemometric data of the database is stored in terms of three instantaneous wind speed components (V_X, V_Y, V_Z) according to the geophysical coordinate system, where V_X is directed from east to west, V_Y is from south to north, and V_Z is vertical, where up is taken to be the positive direction. The long-term continuous monitored wind data considered herein cover 5 years (2013–2017), and are detected simultaneously by all of these ultrasonic anemometers. It is worth noting that the stationarity check and outlier removal are carried out for the initial data, and subsequently those preprocessed data are used for the analysis.

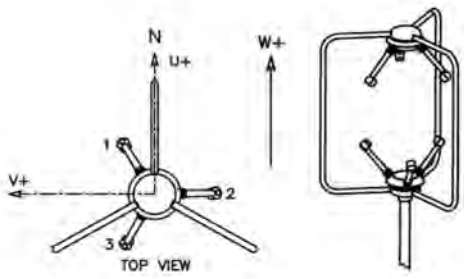

Figure 3. Tri-axial ultrasonic anemometer and the direction of the three instantaneous wind speed components (GILL WindMaster Pro).

3. Statistical Properties of the Wind Speed and Direction

As described above, the measured data detected by the ultrasonic anemometers on the Beijing 325 m high meteorological tower in 2013–2017 are used herein, and the preliminary evaluation of the local statistical properties of the wind speed are carried out first. In total, there are 229,488 10-min length segments of wind records related to each anemometer; they were considered reliable for the following analyses after a suitable quality control.

3.1. Wind Speed

The information related to the 140 m anemometer is presented in Table 2, illustrating the number of the records belonging to different classes of the horizontal 10-min mean wind velocity $\overline{U}$. The 10-min mean wind speed $\overline{U}$ for most of the records (95%) is smaller than 8 m/s. The number of records with the 10-min mean wind speed in the range between 8 m/s and 11 m/s is 8886. The wind records with a mean wind speed larger than 11 m/s are surely neutral and more than two thousand (0.88%).

Table 2. Classes of membership of the 10-min mean wind velocity $\overline{U}$.

$\overline{U}$ (m/s)	$0 < \overline{U} \leq 8$	$8 \leq \overline{U} < 11$	$11 \leq \overline{U} < 20.5$
Number of records	218,590	8886	2012

The designing wind speed is analysed assuming the occurrence of meteorological phenomena corresponding to extreme cyclones. The wind speeds documented in these types of cyclones tend to be very high, and the atmospheric properties tend towards neutrality [34].

The Richardson number, $R_{B,}$ is the common indicator adopted to examine the effect of atmospheric stratification; it is calculated by means of the measurements carried out at two heights, z_1 and z_2, and is given below [35]:

$$R_B = \left(\frac{g}{\overline{\theta}}\right)\frac{\Delta\theta}{\Delta z}\Big/\left(\frac{\Delta U}{\Delta z}\right)^2 \quad (1)$$

in which g is the acceleration due to gravity, and $\Delta z = z_2 - z_1$, $\Delta\theta = \theta_{z_2} - \theta_{z_1}$ and $\overline{\theta}=(\theta_{z_2} + \theta_{z_1})/2$ are the averaged potential temperature at the z_1 and z_2 heights. In this atmospheric environment, it can be found that the potential temperature θ is almost the same as the temperature T measured by the anemometer, such that the former can be substituted by the latter in the computation. When $R_B > 0$, the atmosphere can be considered as stably stratified; when $R_B = 0$, it is neutrally stratified; when $R_B < 0$, it is unstably stratified.

Herein, only the wind records with mean wind speeds higher than 11 m/s at 140 m were used to evaluate the atmospheric stratification condition. In this case, based on the measurements at $z_1 = 47$ m and $z_2 = 140$ m, R_B is in a range between -0.023 and 0.021. Most of the values are zero or slightly larger than 0, such that the atmosphere can be considered to be neutrally stratified. Figure 4 shows the histogram of the mean wind speed values; around half of them are between 11 m/s and 12 m/s. About 1/4 of the data are in the range between 12 m/s and 13 m/s. Then, the number of wind records decreases rapidly with the increase of the mean wind speed.

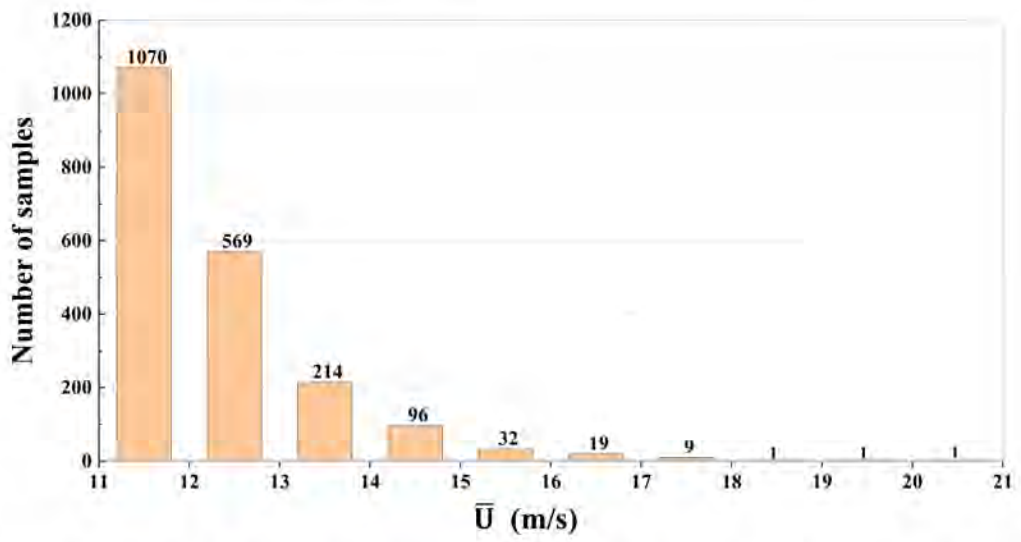

Figure 4. The distribution of the intense wind records with the 10-min mean wind speed detected by the 140 m anemometer.

Based on Figure 4, there are only three records with a 10-min mean wind speed larger than 18 m/s at 140 m, which are 19.24 m/s at 22:40, 5 May 2016; 18.53 m/s at 8:40, 5 May 2017; and 20.47 m/s at 9:20, 5 May 2017, respectively. It can be noted that all of them occurred in May, namely in spring, and this is consistent with the statistical climatological data according to which the most frequent gales happen in spring [25,36]. Besides this, there was a blue alert on 5 May 2016 and a yellow alert on 5 May 2017 for the intense winds in Beijing, which further confirms the occurrence of the strong storm. Luckily, the one detected in 2016 occurred during the night, and no injuries were recorded. On the other hand, on 5 May 2017, some disasters caused by the intense windstorm occurred, as shown in Figure 1, which testifies to the importance of the study about the local wind field.

The data recorded in the period from 2013 to 2017 by the 140 m anemometer installed on the Beijing meteorological tower were used to preliminarily evaluate the local statistical properties of the wind speed in order to avoid the interference of the airflow around the meteorological tower due to the complex urban surroundings. Accordingly, as shown in Figure 5, the distribution of the monthly maximum mean wind speeds in 1-s, 3-s, 1-min and 10-min time intervals for the 5 years extracted from this anemometer are presented. In spring, the peak value of the monthly maximum average wind speed averaged on different time intervals generally appeared in May, and only in 2015 did it occur in April, in correspondence with an intense sandstorm. Then, the mean wind speed presents an obvious decrease in summer. Of particular interest is the summer in 2016. After the investigation, a short intense gust front in June and a thunderstorm in July happened and were detected, which made clear the mean wind speed increasing in short intervals. The monthly maximum average wind speed related to September is relatively smaller, and presents a peak in October or November in autumn. In winter, the monthly maximum average wind speed is generally homogeneous. The abnormal small values in November 2015 and January 2016 probably derive from the lack of valid data due to equipment failure. The annual variation is because of Beijing's closer proximity to the wind source in the spring and winter months [36]. The analysis results are also consistent with the characteristics of the temperate continental monsoon climate in Beijing [37].

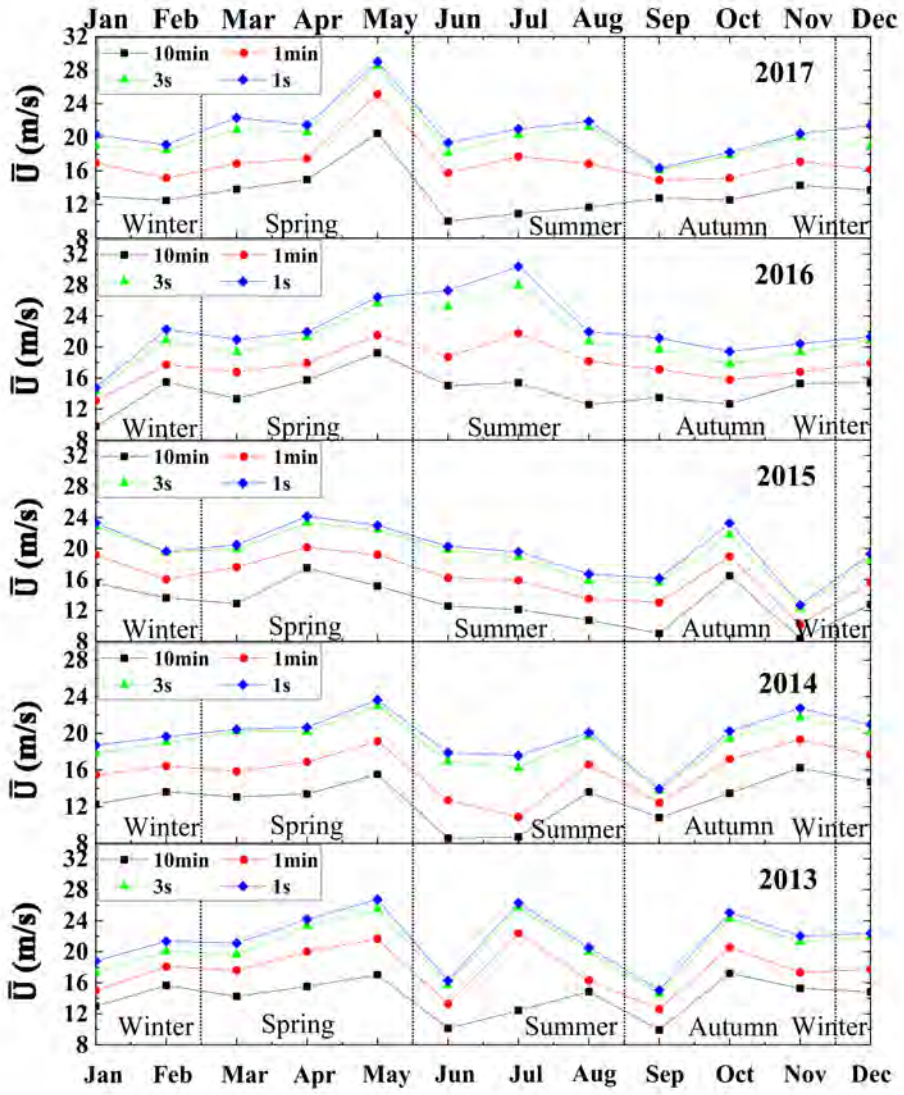

Figure 5. The distribution of the monthly maximum mean wind speeds with different time intervals related to the 140 m anemometer from 2013–2017.

The statistical results of the monthly maximum 10-min mean wind speed, with similar patterns of variation at three levels—namely 47 m, 140 m and 280 m—are shown in Figure 6a. The magnitude of the mean wind speed increases with the increase of the height, which is consistent with the conventional property of the wind profile of synoptic winds. Besides this, the corresponding monthly maximum 3-s gust wind speed related to these three anemometers is also illustrated in Figure 6b. In general, the monthly maximum 3-s gust wind speed presents a tendency to increase with the height. It may be noted that the trend lines related to 140 m and 280 m are very close in some months (orange triangles). In the investigation, all of the special situations which occurred correspond to the same intense wind storms. Furthermore, the abnormal vertical mean wind speed distribution, where the gust wind speed at the height of 140 m even exceeds the wind speed at the height of 280 m (green squares), can be associated to a short-duration wind storm in March and June 2015, and a convective thunderstorm in August 2017. Then, it can be seen that the maximum gust wind speeds at the heights of 47 m and 140 m are very close in June 2014 and April 2017 (black circles), when the thunderstorm and a near gale with a Beaufort scale 7 rating occurred.

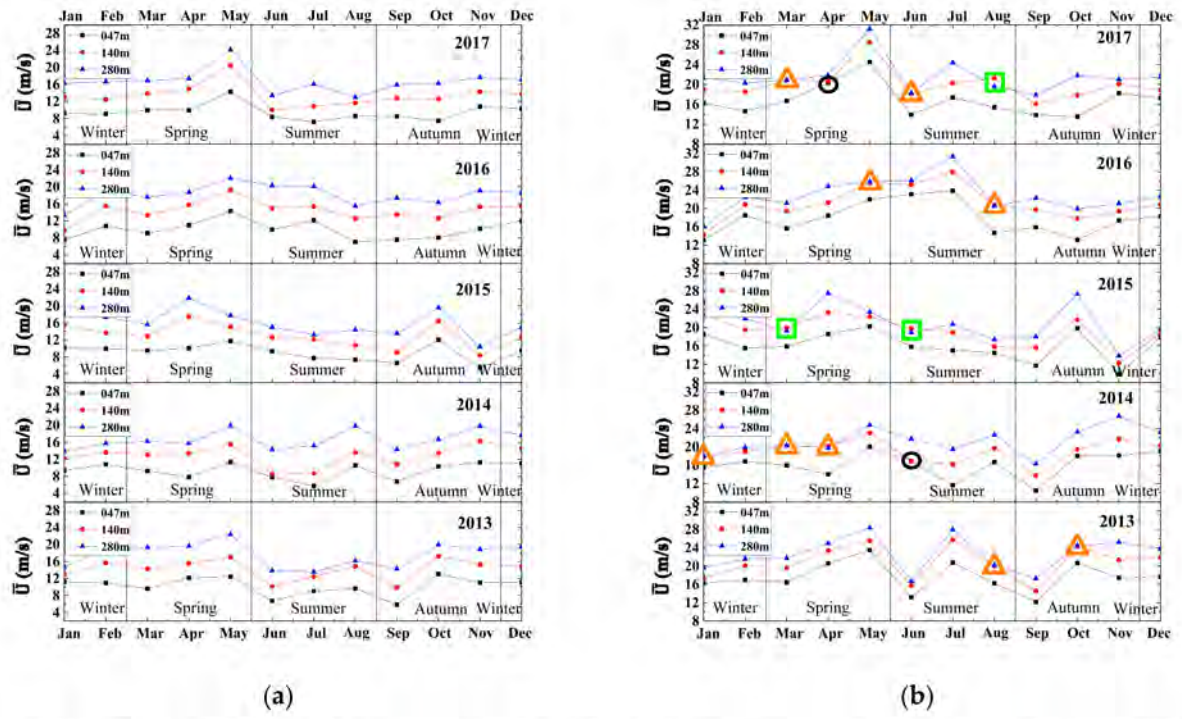

Figure 6. Distribution of the monthly maximum wind speed with time intervals of 10 min (**a**) and 3 s (**b**) from 2013–2017. Orange triangles: the trend lines related to 140 m and 280 m are very close; green squares: the gust wind speed at the height of 140 m even exceeds the wind speed at the height of 280 m. Black circles: the maximum gust wind speeds at the height of 47 m and 140 m are very close.

3.2. Wind Direction

As for the analysis of the mean wind directions, the relevant horizontal wind rose is first presented in Figure 7a based on the 5-year data detected by the 140 m anemometer. It shows that the dominant wind directions are northwest, north, southwest and south. The samples of high wind speeds in the northwest and low wind speeds in the south are relatively numerous, while the samples for the other directions are relatively sparse. The seasonal distribution of the wind direction is illustrated in Figure 7b, which shows that the northwest wind prevails in winter and the southwest wind is dominant in summer. Spring and autumn are the transition seasons, and south, southwest and northwest are the dominant wind directions.

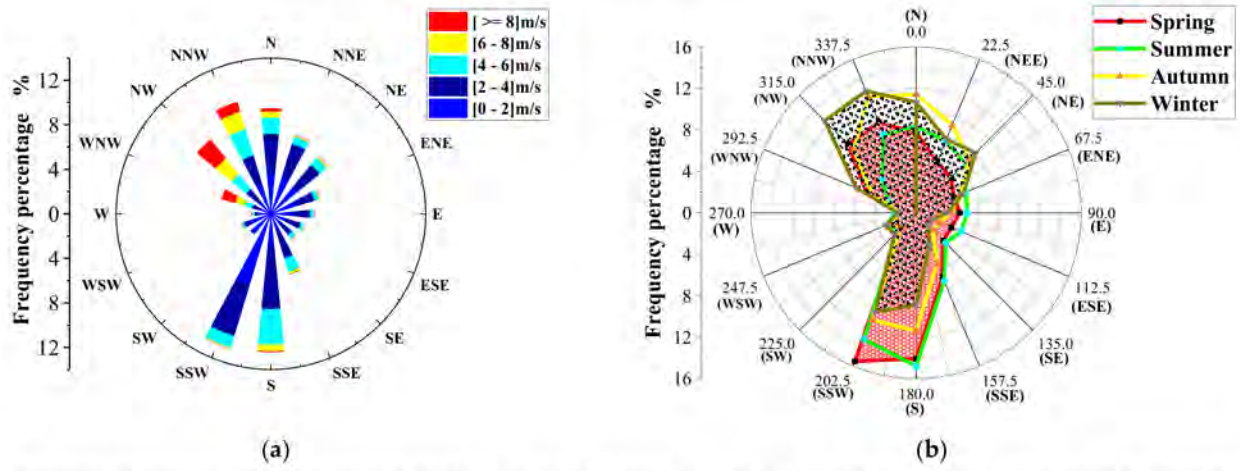

Figure 7. Horizontal wind roses based on the data at 140 m from 2013 to 2017: wind speed distribution (**a**) and seasonal distribution (**b**).

As shown in Table 1, the number of the samples with mean wind speeds higher than 11 m/s is 2012, which is enough for a statistical analysis to be carried out, assuming that the wind speed is associated with the neutral properties of synoptic events [5,6] and thus related to the wind-resistant design of structures.

Furthermore, the wind rose diagram in the four seasons related to the records characterized by mean wind velocities higher than 11 m/s during the period of study from the 140 m anemometer is presented in Figure 8. It shows the dominance of occurrences in the WNW and NW. Intense winds frequently occur in spring, and secondly in winter and autumn, while the wind samples in summer are much smaller than those in the other seasons.

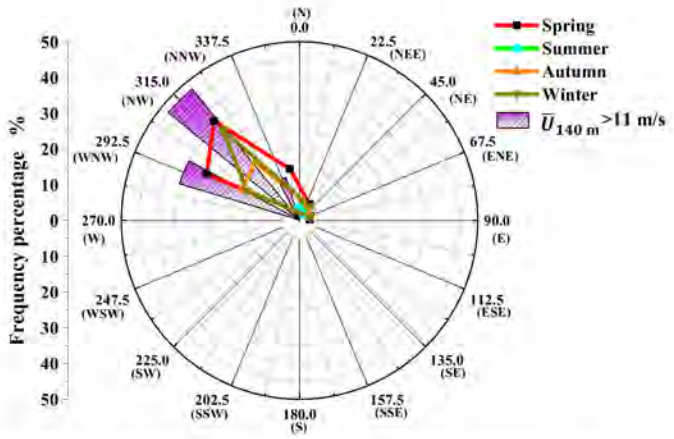

Figure 8. Wind rose diagram in different seasons based on the intense wind records at 140 m from 2013 to 2017.

4. Statistical Properties of the Wind Profiles

For the estimation of the wind profile properties in the Beijing urban area, two intense synoptic wind events which occurred in autumn and spring were first taken as an example and separately illustrated in detail in Sections 4.1 and 4.2. Then, the statistical analysis of a family of wind profiles corresponding to intense synoptic wind records was carried out and examined in Section 4.3.

4.1. Analysis of the Intense Wind Event which Occurred on 10 October 2013

First of all, the synoptic event detected on 10 October 2013 was selected as representative of the intense synoptic winds that occur in Beijing during the autumn. In this case, the Beijing meteorological bureau issued a blue alert for strong winds and there was blown sand in some areas.

Three groups of measured data, recorded at 47 m, 140 m and 280 m heights, were compared in order to investigate the time histories of the 10-min mean wind speed $\overline{U}$ (a), the mean wind direction $\overline{\vartheta}$ (b), the mean temperature $\overline{T}$ (c) and the friction velocity normalized by the mean wind speed $u^*/\overline{U}$ (d) at various altitudes, as shown in Figure 9. The friction velocity u^* can be determined by the formula $u^* = \left[\left(-\overline{u'w'}\right)^2 + \left(-\overline{v'w'}\right)^2\right]^{0.25}$, where $-\overline{u'w'}$ and $-\overline{v'w'}$ are the vertical flux of horizontal momentum, which are obtained from the constant flux layer [38]. The four groups of data from different anemometers fluctuated similarly, which confirms the reliability of the measured data. This synoptic event occurred from about 7:50 Beijing time. The 10-min mean wind speed at 280 m above ground level (AGL) increased from 6.86 m/s to 15.46 m/s suddenly, while the wind speed at 47 m and 140 m increased relatively slowly. At 140 m, the wind speed at 7:50 was 5.05 m/s, and it spent 1 h to reach 13.55 m/s. It increased from 1.12 m/s to 9.09 m/s at 47 m in the same time interval. The high wind speed lasted for about 13 h between the vertical dashed lines. The mean wind speed at 47 m was lighter than that at 140 m and 280 m. As shown in

Figure 9b, the wind directions before and after the storm fluctuated strongly, while they remained stable around 270 deg during the storm. The information on the temperature shows a daily increase in the morning and simultaneously at the beginning of the storm, as illustrated in Figure 9c. Then, the temperature decreased despite the coming noon. It can be inferred that the accumulation of solar energy was the dominant factor for the temperature, while the occurrence of the event affected it slightly. According to Figure 9d, it was found that there were no indications of significant diurnal variations of the dimensionless friction velocity. During the period of strong wind, the patterns of the temporal variations of the dimensionless friction velocity at the three levels were almost the same, which indicates that the atmospheric turbulence is mainly dominated by the mechanical convection, and that the atmosphere is near-neutrally stratified [39].

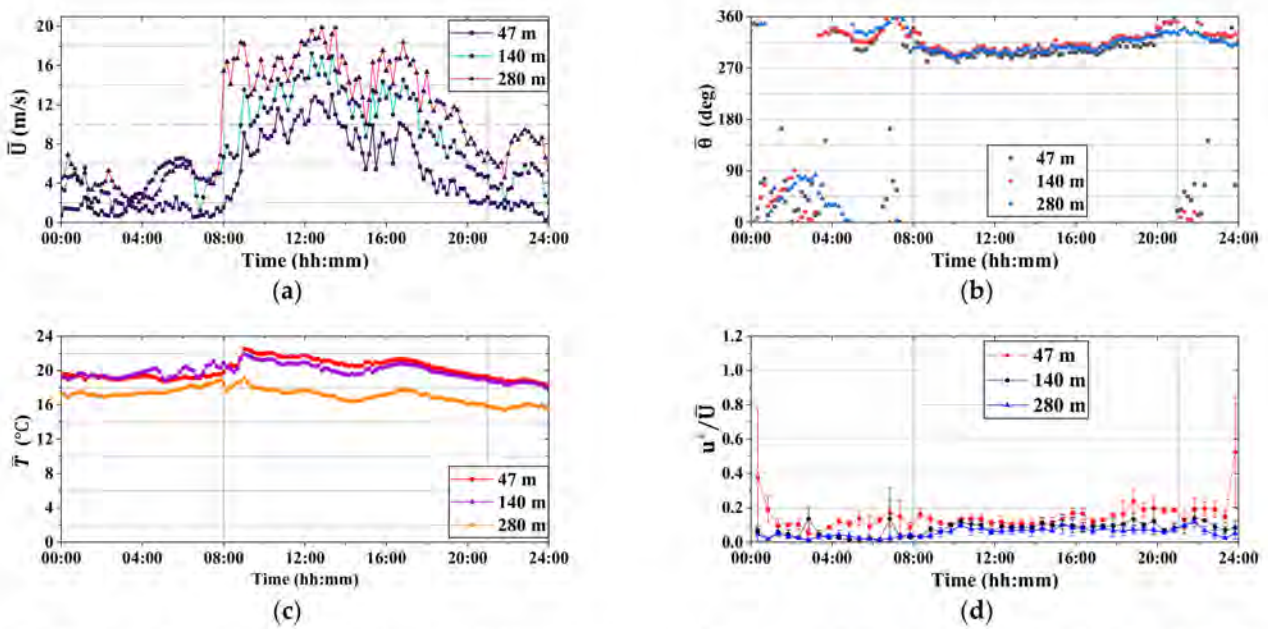

Figure 9. Time histories of the synoptic event which occured on 10 October 2013, related to the heights of 47 m, 140 m and 280 m: (**a**) 10-min mean wind speed, (**b**) 10-min mean wind direction, (**c**) 10-min mean temperature, and (**d**) the friction velocity normalized by the mean wind speed $u^*/\overline{U}$. The vertical dashed lines include the time window of the event.

The two vertical dashed lines drawn in Figure 9 roughly isolate the strong storm event in light of the relatively stable wind direction during this period. Table 3 illustrates the comparison of the maximum, minimum and mean value of the 10-min mean wind speed, the mean wind direction and the mean temperature at the three heights related to the duration between the two vertical lines. The wind speed increases with the height while the temperature decreases as the height increases. Besides this, during this intense wind event, the mean values of the 10-min mean wind direction related to the three heights were almost constant, as shown in Figure 9b, and the difference between the maximum and minimum was mainly due to the beginning and end of the storm.

Table 3. Comparison of the wind data of three heights related to the duration between the two vertical lines in Figure 9.

h (m)	Speed (m/s)			Direction (deg)			Temperature (°C)		
	Max	Min	Mean	Max	Min	Mean	Max	Min	Mean
47	13.03	1.52	7.23	360	280.8	302.1	22.54	19.29	20.91
140	17.22	4.64	11.12	352	291.5	312.2	21.93	18.78	20.08
280	19.92	6.27	14.57	336	287.4	306.5	19.11	15.79	17.21

The profile variations of the 10-min mean wind speed $\overline{U}$ (a), horizontal direction $\overline{\alpha}$ (b) and wind angle of attack $\overline{\gamma}$ (c) (namely the angle between the wind flow direction and the horizontal direction) every two hours are shown in Figure 10. A regular variation trend occurs during the strong storm. The vertical angle changed slightly at low heights and remained almost constant at higher levels.

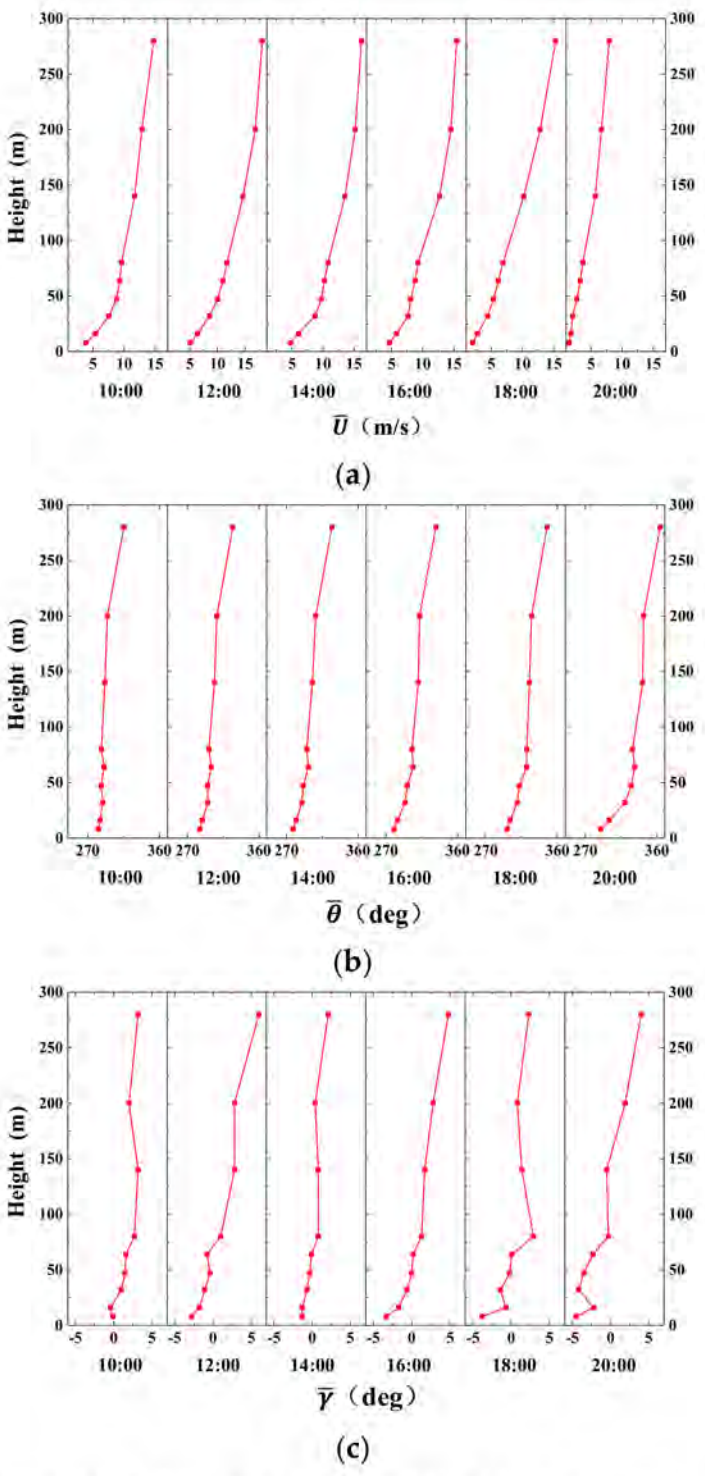

Figure 10. The profile variation of the 10-min mean wind speed (**a**), hotizontal direction (**b**) and wind angle of attack (**c**) on 10 October 2013.

The profiles of the 10-min mean wind speed (a), horizontal direction (b) and wind angle of attack (c) related to some intense wind records during the synoptic event which occurred on 10 October 2013 are shown in Figure 11. It should be noted that the mean wind speeds are normalized with reference to the values detected by the 280 m anemometer. The wind speeds always increase with the increasing height, and their variation tendency is similar. The mean direction remains in the range between 270 and 320 degrees, and appears a little bit clockwise rotated with the increase of the height, followed by a relatively larger clockwise rotation from 200 m to 280 m. This rotation is consistent with the Ekman spiral concepts. When evaluating the measurements up to 300 m in a city center, the Ekman spiral may appear at over 200 m. Most of the wind angle of attacks were negative, namely upward for the lower heights, while for higher heights almost all of them were positive, namely downward. The magnitudes of all of them were small.

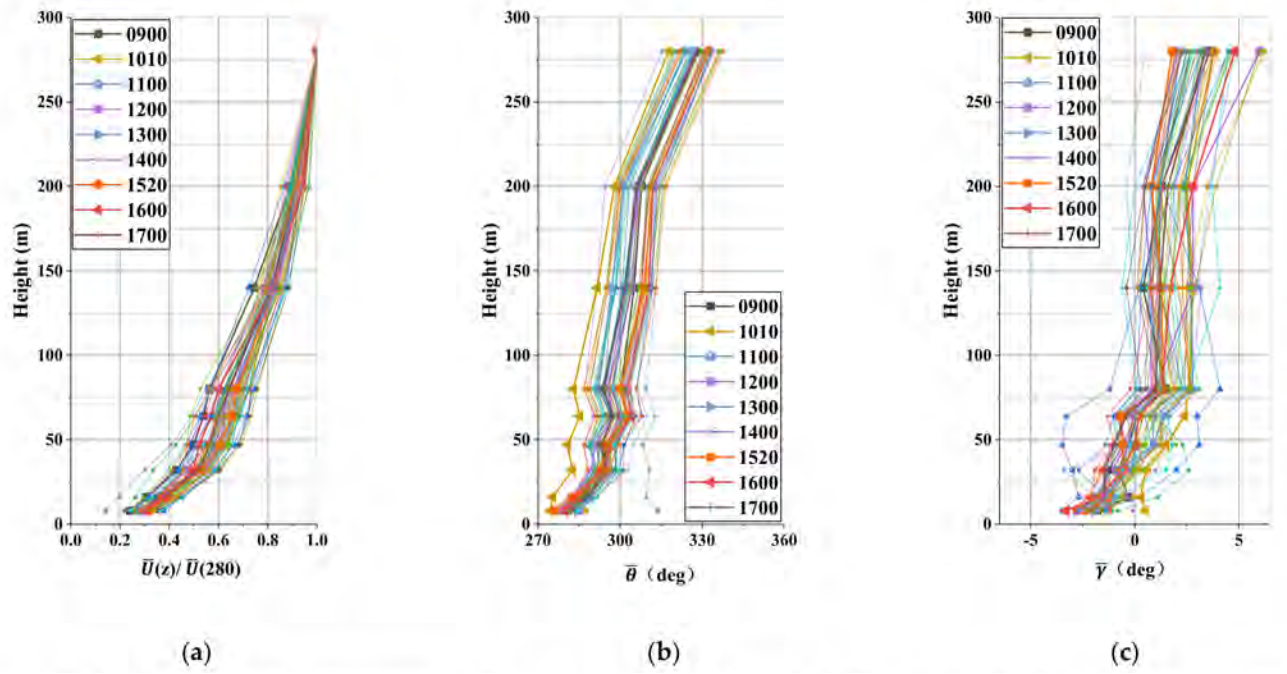

Figure 11. The profiles of 10-min mean wind speed normalized by the value at 280 m (**a**), the horizontal direction (**b**) and the wind angle of attack (**c**) related to the strong wind records of a synoptic event which occured on 10 October 2013.

4.2. Analysis of the Intense Wind Event which Occurred on 5 May 2017

The synoptic event detected on 5 May 2017 was selected as being representative of the intense synoptic winds that occur in Beijing during the spring. Figure 12 shows the 10-min mean wind speed (a), wind direction (b), temperature (c) and normalized friction velocity (d) history related to the heights of 47 m, 140 m and 280 m. The three groups of data also present striking similarities. Besides this, Table 4 reports the maximum, minimum and mean values of the wind speed, wind direction and temperature at the three heights during the period between the two vertical dashed lines in Figure 12. This synoptic event occurred at 7:30 Beijing time and lasted for about 11.5 h. The mean wind speed at 47 m is smaller than that at 140 m and 280 m. As shown in Figure 12b, differently, the wind directions before and after the storm fluctuate strongly at 47 m, and take values around 190 deg at 140 m and around 260 deg at 280 m. Moreover, the directions become about 290 deg at 47 m and 140 m, and about 330 deg at 280 m during the event, as illustrated in Table 3, which is different from the event shown in Figure 9b, proving the individual variation of different synoptic storms. As shown in Figure 12c, the information of the temperature shows an abnormal decrease in the morning when the event occurred, which means that the occurrence of the storm influenced it. Figure 12d shows the temporal variation of the friction velocity normalized with reference to the mean wind speed at three

levels. When the wind speed is low, the fluctuations of the dimensionless friction velocity increase significantly and its statistical characteristics become unsteady. During the strong storm, the normalized friction velocity was almost constant, similar to the event which occurred on 10 October 2013. The further and detailed study of the stratified structure of the atmospheric boundary layer of the Beijing urban area is still in progress.

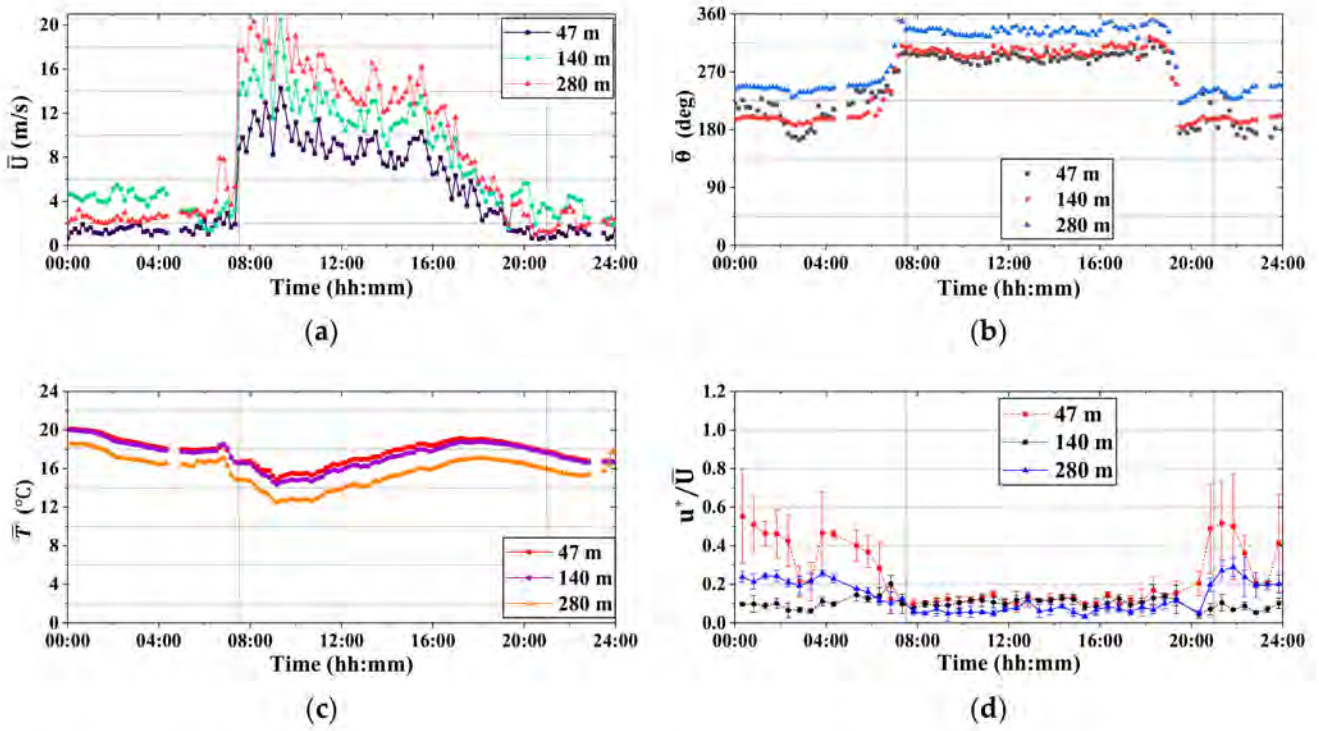

Figure 12. The 10-min mean wind speed (**a**), wind direction (**b**), temperature (**c**) and friction velocity normalized by the mean wind speed $u^*/\overline{U}$, (**d**) history of the synoptic event which occured on 5 May 2017, related to the heights of 47 m, 140 m and 280 m.

Table 4. Comparison of the wind data of three heights related to the duration between two vertical lines in Figure 12.

h (m)	Speed (m/s)			Direction (deg)			Temperature (°C)		
	Max	Min	Mean	Max	Min	Mean	Max	Min	Mean
47	14.29	2.31	8.17	339.3	280.8	298.14	19.13	14.86	17.27
140	20.47	3.75	11.3	339.3	291.5	309.02	18.79	14.35	16.76
280	24.2	4.49	13.86	354.5	287.4	304.68	17.08	12.48	14.85

The profile variations of the 10-min mean wind speed (a), horizontal direction (b) and wind angle of attack (c) every two hours are illustrated in Figure 13. Similarly to the previous event, during the storm the shapes of the wind speed and wind direction profiles change a little as time goes on. In particular, the wind direction presents a relatively large clockwise rotation from 200 m to 280 m, which is the same as the event which occurred on 10 October 2013; furthermore, in this case the generation of the Ekman spiral may explain this phenomenon. As far as concerns the wind angle of attack, it varies a little bit with the time during the intense event; moreover, it exhibits a positive and negative change for the lower levels whilst remaining relatively constant for the higher levels.

The profiles of $\overline{U}$ normalized with reference to the value at 280 m (a), the horizontal direction (b) and the wind angle of attack (c) are shown in Figure 14. The wind speed profiles of the different 10-min length segments present a relatively similar trend to the height. This property is more prominent for the wind direction, which rotates clockwise

a little. As far as concerns the angle of attack, most of the values lower than 64 m are negative. They then become relatively constant until 200 m. It is noteworthy that there is a slight increase between the heights of 200 m and 280 m.

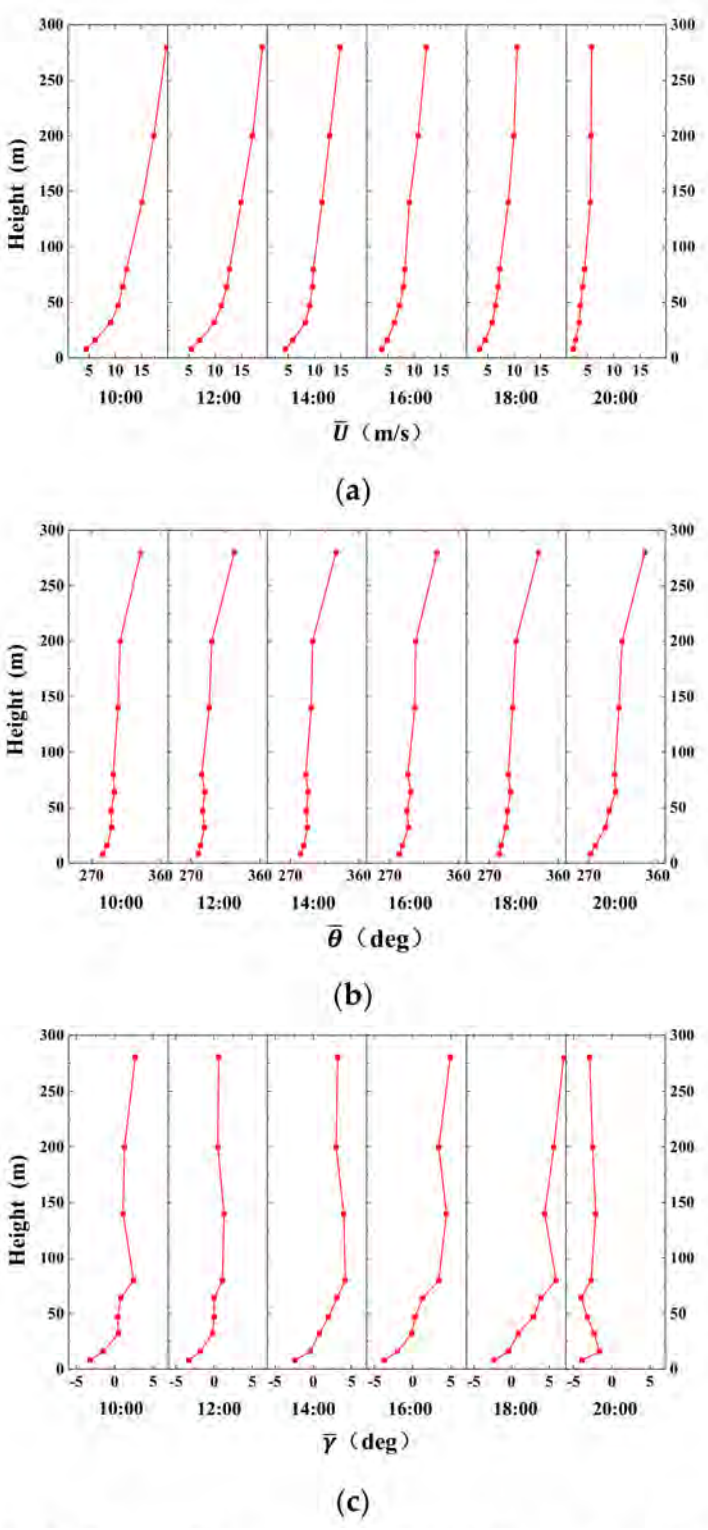

Figure 13. The profile variation of the 10-min mean wind speed (**a**), hotizontal direction (**b**) and wind angle of attack (**c**) of the synoptic event which occured on 5 May 2017.

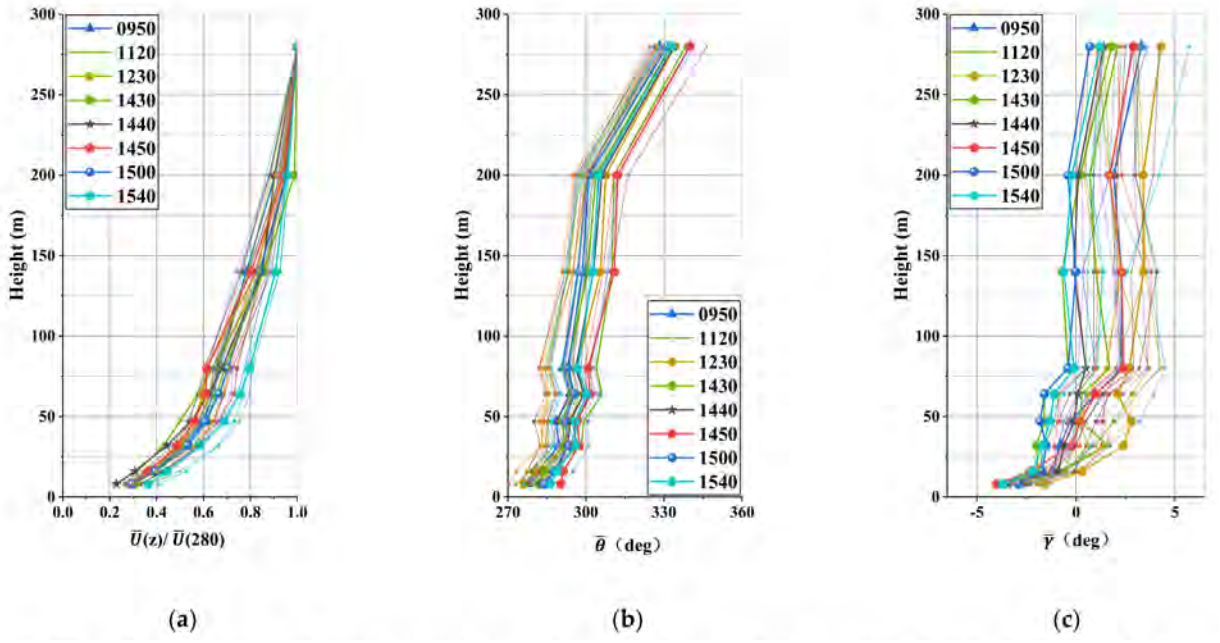

Figure 14. The profiles of the 10-min mean wind speed nomalized by the related value at 280 m (**a**), the horizontal direction (**b**) and the wind angle of attack (**c**) related to the strong wind records of the synoptic event which occured on 5 May 2017.

4.3. Statistical Analysis of the Intense Wind Speed Records

Estimating the 5-year measured data, eight intense wind speed samples were selected to show a preliminary tendency of the wind speed (a), wind direction (b) and wind angle of attack profiles (c); they are shown in Figure 15. The mean wind speeds at 280 m corresponding to these records were between 16.8 m/s and 24.2 m/s; besides this, they were extracted from 6 different storms.

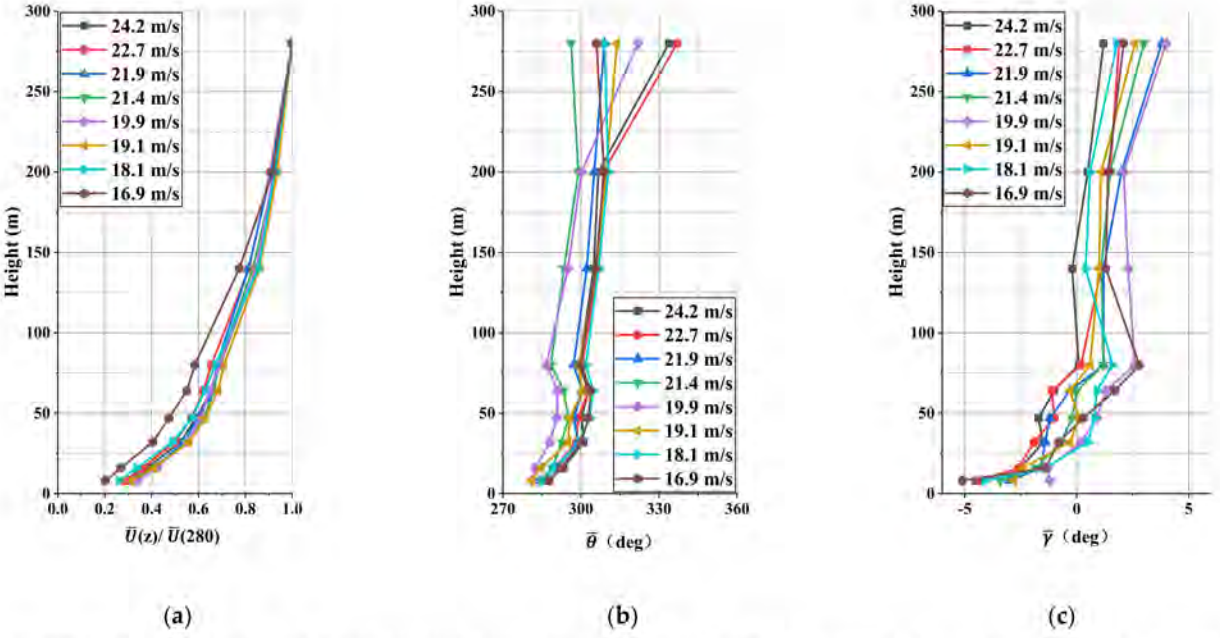

Figure 15. The profiles of the 10-min mean wind speed nomalized by the related value at 280 m (**a**), the horizontal direction (**b**) and the wind angle of attack (**c**) related to eight strong synoptic wind records.

Figure 15a shows that the changes of the mean wind speeds with the height of the different samples are very close. According to Figure 15b, the mean wind direction rotates

clockwise a little bit with heights under 200 m, while above 200 m the direction rotates clockwise relatively greatly with the height; this situation is consistent with the two events described above and the Ekman spiral in the Northern Hemisphere. Besides this, the wind angle of attacks of the samples are negative, as shown in Figure 15c for the lower heights. From 80 m to 200 m, most of them are positive, and remain around constant values with the height. Then, they increase slightly from 200 m to 280 m. It may be preliminarily inferred that this might be due to the stratified structure of the atmospheric boundary layer, which deserves further analysis.

For the assessment of the wind loads on structures in the Chinese code (GB50009-2012), the representation of the mean wind velocity profile by the power law [40,41] is first investigated. It can be written as

$$U(z) = U_r \cdot \left(\frac{z}{z_r}\right)^{\alpha} \quad (2)$$

in which $U(z)$ is the mean wind speed at the height z AGL, U_r is the mean wind speed at the reference height z_r AGL, and α is the ground roughness exponent. The estimation of the past study indicated that the measured data from the anemometers below 47 m are influenced by the buildings around the meteorological tower [25]. Here, the intense wind speed data from the anemometers above 47 m were adopted for the fitting of the wind speed profile by the least square method.

Here, the distribution of the ground roughness exponents α obtained from all of the considered intense records with 10-min mean wind speeds faster than 11 m/s related to the 140 m anemometer by regression analysis is presented in Figure 16. Accordingly, it can be found that most of the results, namely 60.4%, are between 0.2 and 0.4. Then, the profiles are separated into five different families with different wind speed ranges at 140 m height: $11 \leq \overline{U} < 12$, $12 \leq \overline{U} < 13$, $13 \leq \overline{U} < 14$, $14 \leq \overline{U} < 15$, and $15 \leq \overline{U} < 21$ m/s. The fitting ground roughness exponents of every record belonging to the same family are averaged and illustrated in Table 5, below. As the mean wind speed of the records considered increases, the ground roughness exponent decreases gradually. All of the average fitting exponents are larger than the maximum value in the Chinese National Load Code (α = 0.30 for terrain D). On the other hand, based on the code, the ground roughness exponent around the tower is 0.22 (terrain C), a value lower than the results from the measured data [31].

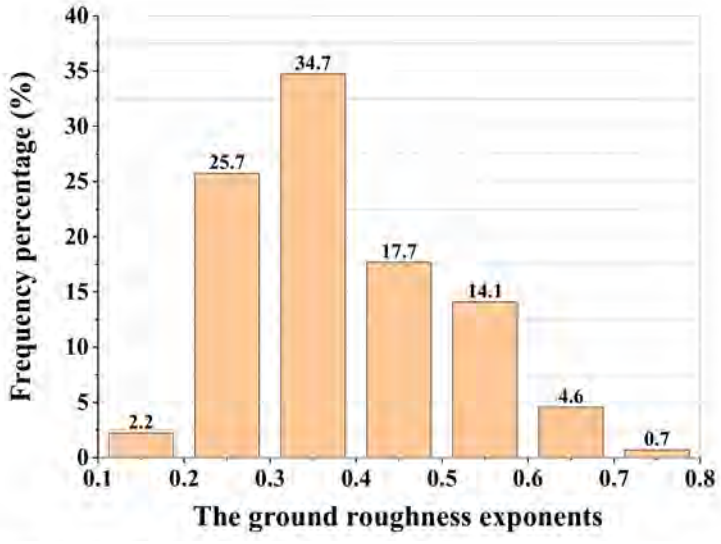

Figure 16. The distribution of the ground roughness exponents.

Table 5. Average fitting ground roughness exponents of every record belonging to the same family.

$\overline{U}$ (m/s)	α
$11 \leq \overline{U} < 12$	0.393
$12 \leq \overline{U} < 13$	0.378
$13 \leq \overline{U} < 14$	0.372
$14 \leq \overline{U} < 15$	0.361
$15 \leq \overline{U} < 21$	0.327

There might be two main reasons for the relatively larger values obtained from the measured data. One is due to the rapid development of the buildings around the Beijing meteorological tower in recent years. The surface roughness has increased and the city's underlying surface has become more complex. Therefore, part of the original rules in the load code are no longer applicable. The other is that in an area with a high density of buildings, the height at which the mean velocity approaches zero is not the terrain level but the average height of the obstacles, namely the zero plane displacement. This condition is not considered in the power law profiles adopted in the Chinese load code, which makes the obtained ground roughness exponents α larger.

In addition to the power law, the log law also is investigated below for the description of the vertical distribution of the mean wind speed in the ABL. According to the asymptotic similarity considerations for a neutral atmospheric boundary layer [42,43], it is given by:

$$U(z) = \frac{u^*}{\kappa} \cdot ln\left(\frac{z}{z_0}\right) \tag{3}$$

in which u^* is the surface friction velocity; κ is von Karman's constant, assumed here to be 0.4; and z_0 is the surface roughness length. When considering a dense canopy with packed surface obstacles such as vegetations and buildings, the mean flow does not penetrate downward to the surface; therefore, Equation (3) is corrected as

$$U(z) = \frac{u^*}{\kappa} \cdot ln\left(\frac{z-d}{z_0}\right) \tag{4}$$

where d is the zero plane displacement.

However, some previous research has shown that the log law does not represent the mean wind speed profile well for the higher levels, typically for $z > 200$ m [11,13,44]. The Deaves–Harris model (D-H model) incorporates more of the real physics of the ABL meeting both the upper and lower boundary conditions, and is supposed to be applicable to the entire boundary layer [45]. It is expressed as:

$$U(z) = \frac{u^*}{\kappa}\left[ln\left(\frac{z}{z_0}\right) + 5.75\left(\frac{z}{h}\right) - 1.88\left(\frac{z}{h}\right) - 1.33\left(\frac{z}{h}\right)^2 + 0.25\left(\frac{z}{h}\right)^4\right] \tag{5}$$

in which h is the height of the ABL, and is given by:

$$Uh = \frac{u^*}{Bf} \tag{6}$$

where f is the Coriolis parameter equaling to $9.375 \times 10^{-5} s^{-1}$ and B is an empirical constant, of which the magnitude is 6 according to the observed wind profiles [14].

The measured profiles which are the ensemble-averaged values of the 10-min mean wind speed for the whole family considered (a) and several regimes of the reference wind speed at 140 m AGL ((b)–(f)) are compared with the empirical mean speed profiles which were determined based on the aerodynamic parameters fitted by the corresponding measurement in Figure 17. All of the profiles were normalized at the 140 m value. The average values of u^* at 80 m, where the maximum occurs in the near-surface layer, were

applied in these models [11,46]. The concept of a local u^* value depending on height above the ground was also used by Burlando et al. [47] with reference to complex terrains.

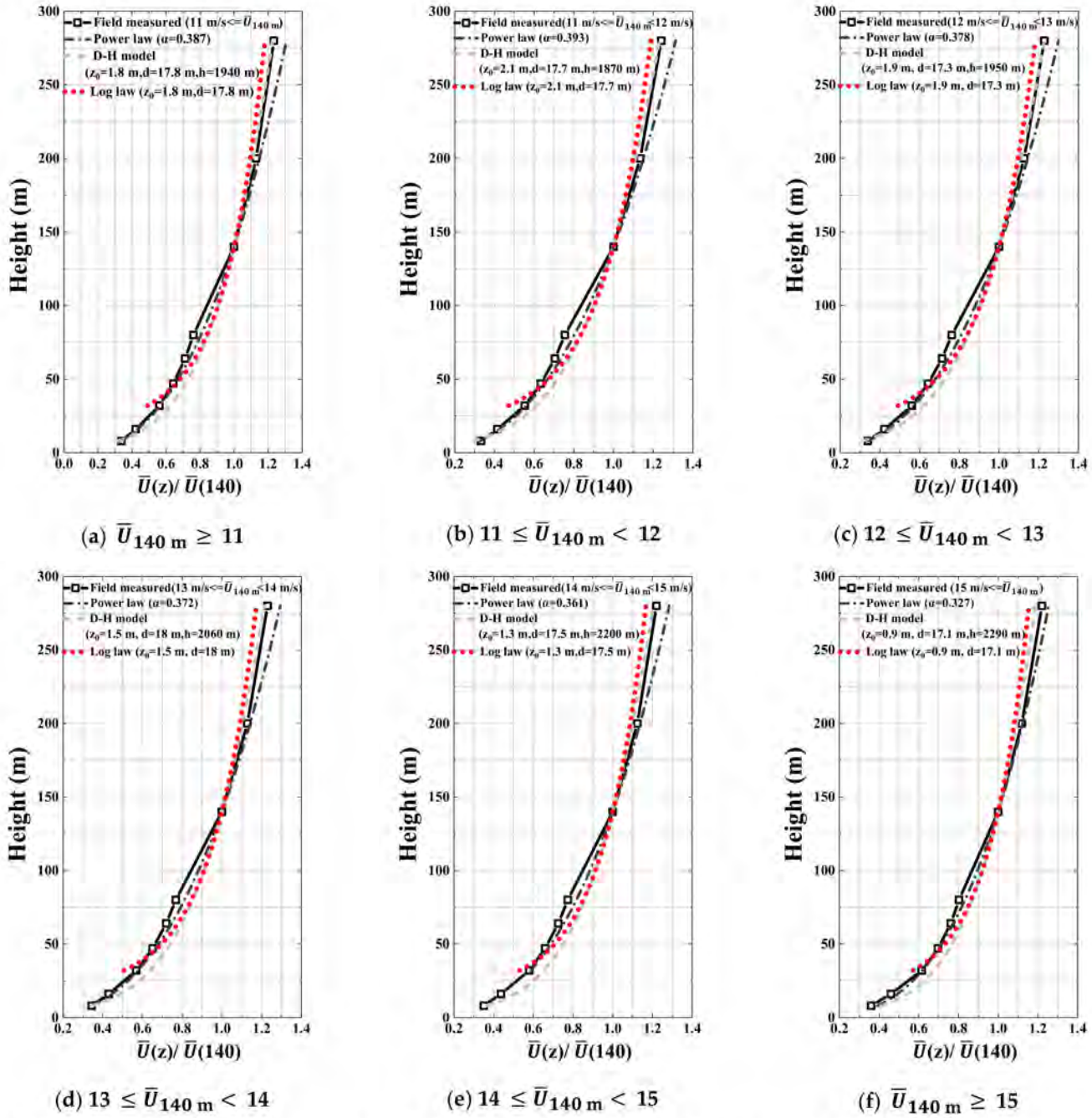

Figure 17. Comparison of the measured mean wind speed profile with those of the empirical models based on the adoption of the measured parameters related to wind records with different speed ranges (m/s).

The profiles of the power law and log law are in closer agreement with the measured profiles for the lower heights. Besides this, for higher levels, the power law exhibits significant differences with the measured data, whereas the log-law model underestimates the wind speeds; however, the corrected log law based on the D–H model presents a good fit to the measured mean wind speed profiles. The roughness length z_0 and zero-plane displacement d are 1.8 m and 17.8 m for the ensemble, respectively. Besides this, the former decreases gradually with the increase of the wind speed period calculated and the latter does not present a clear rule for the moment. The height h of the neutral ABL based on

the D–H model is 1940 m, corresponding to the whole family considered, which exceeds greatly the gradient height (450 m) recommended by the code (GB50009-2012) [33]. It is observed that the value h generally increases with the wind speed. All of the traditional laws of wind profiles based on open and flat terrains are not appropriate for the UABL wind and could only present appropriate fitting. It is necessary to take account of the aerodynamic characteristic parameters of UABL based on a vertical stratified structure for the wind profiles in the urban boundary layer.

5. Conclusions

The 325 m meteorological tower in Beijing provides a good opportunity to detect high-resolution measured data at different levels using a refined analysis of UABL. The properties of the measurement site and anemometers on the tower were illustrated here for the first time. Then the database generated by it based on nine ultrasonic anemometers mounted at different heights from 8 m to 280 m along the tower from 2013 to 2017 was estimated, after which a total of 229,488 10-min length segments of wind speed records related to each anemometer were retained and considered to be reliable after a suitable quality control for further analyses.

In order to display a preliminary viewpoint on the wind-climate properties in the Beijing urban area, the statistical properties of the wind speed and direction were evaluated. It was found that, generally, the season with the most frequent gales is spring. Moreover, most of the high wind speed records are from the northwest, and the low wind speed records are from the south. The seasonal distribution of the wind direction was also presented, and it was found that the northwest wind prevails in winter, the dominant direction in summer is southwest, and spring and autumn can be considered as transition seasons.

Then, as for learning the property of wind profiles in the Beijing urban area, eight intense wind speed samples were preliminarily examined. It is worth noting that the wind speed profiles related to all of them exhibit a similar growth with the height. As the height increases, the mean wind direction shows a small amount of clockwise rotation with heights under 200 m, while it rotates counterclockwise from 200 m to 280 m, which might be owing to the Ekman spiral. With the increase of the measured data, this deserves further study. Besides this, the wind angle of attacks of the samples are negative for the lower levels, then become positive and almost hardly vary with height. In particular, from 200 m to 280 m, there is a slight increase of the wind angle of attack.

Then, the intense wind speed segments were selected herein for the further study of the wind speed profiles. The corresponding wind speed profiles related to different wind speed ranges were fitted by applying the power law. The ground roughness exponent decreases gradually with the increase of the wind speed. Furthermore, compared with the Chinese National Load Code (GB50009-2012), the average fitting exponents obtained by the measurements are larger than the proposed value for the site around the tower in the code ($\alpha = 0.22$ for terrain C). This means that the empirical model underestimates the influence of the ground roughness, which probably is due to the lack of measured data within a certain height range of the urban center. Besides this, it was found that, for the lower heights, the power-law and log-law profiles agree with the measured profiles. For higher heights, the power-law profiles present significant differences from the measured data: the log-law model underestimates the wind speeds, whereas the log law correction based on the D–H model improves the matching, providing a good fit to the measured profiles. The inaccuracy of traditional laws of wind profiles which can be found when fitting the UABL wind and the aerodynamic characteristic parameters of UABL based on vertical stratified structures have to be taken into account. Further research is necessary for the safety, reliability and economy of building structures.

The results were collected by ultra-sonic anemometers and pertain to the Beijing urban area, where buildings are relatively dense. The acquisition of new data through other instruments, like LiDAR (light detection and ranging), may strongly contribute

to refining the study of the wind-speed profile carried out here, and may consequently contribute to the improvement of current engineering standards.

The study of the property of turbulence is a matter for another paper currently in progress.

Author Contributions: Conceptualization, S.Z. and B.L.; methodology, S.Z.; software, X.Z.; formal analysis, X.X.; data curation, X.Z. and S.Z.; writing—original draft preparation, S.Z.; writing—review and editing, G.S. All authors have read and agreed to the published version of the manuscript.

Funding: This work was funded by the National Natural Science Foundation of China (51878041), a Project supported by Beijing Postdoctoral Research Foundation (2021-ZZ-115) and the Research Ability Enhancement Program for Young Teachers of Beijing University of Civil Engineering and Architecture (X21071). It was also supported by the 111 Project of China (B13002).

Institutional Review Board Statement: Not applicable.

Informed Consent Statement: Not applicable.

Data Availability Statement: Data sharing not applicable.

Conflicts of Interest: The authors declare no conflict of interest.

References

1. Xie, J.; Liao, Z.; Fang, X.; Xu, X.; Wang, Y.; Zhang, Y.; Liu, J.; Fan, S.; Wang, B. The characteristics of hourly wind field and its impacts on air quality in the Pearl River Delta region during 2013–2017. *Atmos. Res.* **2019**, *227*, 112–124. [CrossRef]
2. Yang, Q.; Gao, R.; Bai, F.; Li, T.; Tamura, Y. Damage to buildings and structures due to recent devastating wind hazards in East Asia. *Nat. Hazards* **2018**, *92*, 1321–1353. [CrossRef]
3. Tamura, Y.; Xu, X.; Yang, Q. Characteristics of pedestrian-level Mean wind speed around square buildings: Effects of height, width, size and approaching flow profile. *J. Wind Eng. Ind. Aerodyn.* **2019**, *192*, 74–87. [CrossRef]
4. Roth, M. Review of atmospheric turbulence over cities. *Q. J. R. Meteorol. Soc.* **2007**, *126*, 941–990. [CrossRef]
5. Solari, G.; Burlando, M.; De Gaetano, P.; Repetto, M.P. Characteristics of thunderstorms relevant to the wind loading of structures. *Wind Struct. Int. J.* **2015**, *20*, 763–791. [CrossRef]
6. Zhang, S.; Solari, G.; De Gaetano, P.; Burlando, M.; Repetto, M.P. A refined analysis of thunderstorm outflow characteristics relevant to the wind loading of structures. *Probabilistic Eng. Mech.* **2018**, *54*, 9–24. [CrossRef]
7. Zhang, S.; Solari, G.; Yang, Q.; Repetto, M.P. Extreme wind speed distribution in a mixed wind climate. *J. Wind Eng. Ind. Aerodyn.* **2018**, *176*, 239–253. [CrossRef]
8. Burlando, M.; Zhang, S.; Solari, G. Monitoring, cataloguing, and weather scenarios of thunderstorm outflows in the northern Mediterranean. *Nat. Hazards Earth Syst. Sci.* **2018**, *18*, 2309–2330. [CrossRef]
9. Burlando, M.; Romanić, D.; Solari, G.; Hangan, H.; Zhang, S. Field Data Analysis and Weather Scenario of a Downburst Event in Livorno, Italy, on 1 October 2012. *Mon. Weather. Rev.* **2017**, *145*, 3507–3527. [CrossRef]
10. Zhang, S.; Solari, G.; Burlando, M.; Yang, Q.S. Directional decomposition and properties of thunderstorm out-flows. *J. Wind Eng. Ind. Aerodyn.* **2019**, *189*, 71–90. [CrossRef]
11. Li, Q.; Zhi, L.; Hu, F. Boundary layer wind structure from observations on a 325m tower. *J. Wind Eng. Ind. Aerodyn.* **2010**, *98*, 818–832. [CrossRef]
12. Holtslag, B. Estimates of diabatic wind speed profiles from near-surface weather observations. *Bound. Layer Meteorol.* **1984**, *29*, 225–250. [CrossRef]
13. Tieleman, H.W. Strong wind observations in the atmospheric surface layer. *J. Wind Eng. Ind. Aerodyn.* **2008**, *96*, 41–77. [CrossRef]
14. Tamura, Y.; Iwatani, Y.; Hibi, K.; Suda, K.; Nakamura, O.; Maruyama, T.; Ishibashi, R. Profiles of mean wind speeds and vertical turbulence intensities measured at seashore and two inland sites using Doppler sodars. *J. Wind Eng. Ind. Aerodyn.* **2007**, *95*, 411–427. [CrossRef]
15. Kettle, A.J. Unexpected vertical wind speed profiles in the boundary layer over the southern North Sea. *J. Wind Eng. Ind. Aerodyn.* **2014**, *134*, 149–162. [CrossRef]
16. Shu, Z.; Li, Q.; He, Y.; Chan, P. Observational study of veering wind by Doppler wind profiler and surface weather station. *J. Wind Eng. Ind. Aerodyn.* **2018**, *178*, 18–25. [CrossRef]
17. Gentry, B.M.; Chen, H.; Li, S.X. Wind measurements with 355-nm molecular Doppler lidar. *Opt. Lett.* **2000**, *25*, 1231–1233. [CrossRef]
18. Kent, C.W.; Grimmond, C.; Gatey, D.; Barlow, J.F. Assessing methods to extrapolate the vertical wind-speed profile from surface observations in a city centre during strong winds. *J. Wind Eng. Ind. Aerodyn.* **2018**, *173*, 100–111. [CrossRef]
19. Xu, X.; Yang, Q.; Yoshida, A.; Tamura, Y. Characteristics of pedestrian-level wind around super-tall buildings with various configurations. *J. Wind Eng. Ind. Aerodyn.* **2017**, *166*, 61–73. [CrossRef]

20. Stacey, M.W.; Pond, S.; Leblond, P.H.; Will, H.; Salfeld, J.; Pfaff, E.; Manso, C.; Theilmann, L.; Schaler, H. A Wind-Forced Ekman Spiral as a Good Statistical Fit to Low-Frequency Currents in a Coastal Strait. *Science* **1986**, *233*, 470–472. [CrossRef]
21. Tse, K.T.; Weerasuriya, A.U.; Kwok, K. Simulation of twisted wind flows in a boundary layer wind tunnel for pedestrian-level wind tunnel tests. *J. Wind Eng. Ind. Aerodyn.* **2016**, *159*, 99–109. [CrossRef]
22. Shiau, B.-S.; Chen, Y.-B. In situ measurement of strong wind velocity spectra and wind characteristics at Keelung coastal area of Taiwan. *Atmos. Res.* **2001**, *57*, 171–185. [CrossRef]
23. Román-Cascón, C.; Yagüe, C.; Steeneveld, G.-J.; Sastre, M.; Arrillaga, J.A.; Maqueda, G. Estimating fog-top height through near-surface micrometeorological measurements. *Atmos. Res.* **2016**, *170*, 76–86. [CrossRef]
24. Azorin-Molina, C.; Asin, J.; McVicar, T.; Minola, L.; Lopez-Moreno, I.; Vicente-Serrano, S.M.; Chen, D. Evaluating anemometer drift: A statistical approach to correct biases in wind speed measurement. *Atmos. Res.* **2018**, *203*, 175–188. [CrossRef]
25. Zhang, S.; Yang, Q.; Solari, G.; Li, B.; Huang, G. Characteristics of thunderstorm outflows in Beijing urban area. *J. Wind Eng. Ind. Aerodyn.* **2019**, *195*, 104011. [CrossRef]
26. Li, Q.; Zhi, L.; Hu, F. Field monitoring of boundary layer wind characteristics in urban area. *Wind Struct. Int. J.* **2009**, *12*, 553–574. [CrossRef]
27. Hui, Y.; Li, B.; Kawai, H.; Yang, Q. Non-stationary and non-Gaussian characteristics of wind speeds. *Wind Struct. Int. J.* **2017**, *24*, 59–78. [CrossRef]
28. Solari, G.; Burlando, M.; Repetto, M.P. Detection, simulation, modelling and loading of thunderstorm outflows to design wind-safer and cost-efficient structures. *J. Wind Eng. Ind. Aerodyn.* **2020**, *200*, 104142. [CrossRef]
29. Brusco, S.; Lerzo, V.; Solari, G. Directional response of structures to thunderstorm outflows. *Meccanica* **2019**, *54*, 1281–1306. [CrossRef]
30. Al-Jiboori, M.H.; Fei, H. Surface roughness around a 325-m meteorological tower and its effect on urban turbulence. *Adv. Atmos. Sci.* **2005**, *22*, 595–605. [CrossRef]
31. Government of China. *Load Code for the Design of Building Structures*; National Standard of the People's Republic of China Series GB50009-2012; China Architecture & Building Press: Beijing, China, 2012; pp. 31–32.
32. Liu, J.; Gao, C.Y.; Ren, J.; Gao, Z.; Liang, H.; Wang, L. Wind resource potential assessment using a long term tower measurement approach: A case study of Beijing in China. *J. Clean. Prod.* **2018**, *174*, 917–926. [CrossRef]
33. Zhang, X.X.; Li, B.; Zhang, S.; Yang, Q.S.; Tian, Y.J. Study on the characteristics of wind field in Urban Boundary Layer based on the measured data in Central Beijing. *J. Build. Struct.* **2020**. (In Chinese)
34. Dyrbye, C.; Hansen, S.O. *Wind Loads on Structures*; Wiley: Hoboken, NJ, USA, 1997.
35. Stull, R.B. *An Introduction to Boundary Layer Meteorology*; Springer: Berlin/Heidelberg, Germany, 1988.
36. Liu, J.; Gao, Z.; Wang, L.; Li, Y.; Gao, C.Y. The impact of urbanization on wind speed and surface aerodynamic characteristics in Beijing during 1991–2011. *Meteorol. Atmos. Phys.* **2018**, *130*, 311–324. [CrossRef]
37. Song, X.; Zhang, J.; Zou, X.; Zhang, C.; AghaKouchak, A.; Kong, F. Changes in precipitation extremes in the Beijing metropolitan area during 1960–2012. *Atmos. Res.* **2019**, *222*, 134–153. [CrossRef]
38. Grimmond, C.S.B.; Oke, T.R. Aerodynamic Properties of Urban Areas Derived from Analysis of Surface Form. *J. Appl. Meteorol.* **1999**, *38*, 1262–1292. [CrossRef]
39. Liu, G.; Sun, J.; Jiang, W. Observational verification of urban surface roughness parameters derived from morphological models. *Meteorol. Appl.* **2009**, *16*, 205–213. [CrossRef]
40. Davenport, A.G. The application of statistical concepts to the wind loading of structures. *Proc. Inst. Civ. Eng.* **1961**, *19*, 449–472. [CrossRef]
41. Solari, G. *Wind Science and Engineering: Origins, Developments, Fundamentals and Advancements*; Springer: Cham, Switzerland, 2019.
42. Davenport, A.G. Rationale for Determining Design Wind Velocities. *Struct. Eng. ASCE* **1960**, *86*, 39–68. [CrossRef]
43. Simiu, E.; Scanlan, R.H. *Wind Effects on Structures—Fundamentals and Applications to Design*; John Wiley & Sons Inc.: Hoboken, NJ, USA, 1996; pp. 42–43.
44. Cook, N.J. The Deaves and Harris ABL model applied to heterogeneous terrain. *J. Wind Eng. Ind. Aerodyn.* **1997**, *66*, 197–214. [CrossRef]
45. Deaves, D.; Harris, R. *A Mathematical Model of the Structure of Strong Winds*; Construction IndustryResearch and Information Association Report Series 76; Construction Industry Research and Information Association: London, UK, 1978.
46. Moriwaki, R.; Kanda, M. Flux-gradient profiles for momentum and heat over an urban surface. *Theor. Appl. Clim.* **2006**, *84*, 127–135. [CrossRef]
47. Burlando, M.; Carassale, L.; Georgieva, E.; Ratto, C.F.; Solari, G. A simple and efficient procedure for the numerical simulation of wind fields in complex terrain. *Bound. Layer Meteorol.* **2007**, *125*, 417–439. [CrossRef]